Article

Feed Spacer Geometries and Permeability Coefficients. Effect on the Performance in BWRO Spriral-Wound Membrane Modules

Alejandro Ruiz-García [1,]* **and Ignacio de la Nuez Pestana** [2]

[1] Department of Mechanical Engineering, University of Las Palmas de Gran Canaria, 35001 Las Palmas, Spain
[2] Department of Electronic and Automatic Engineering, University of Las Palmas de Gran Canaria, 35001 Las Palmas, Spain; ignacio.nuez@ulpgc.es
[*] Correspondence: alejandro.ruiz@ulpgc.es; Tel.: +34-928-451-888

Abstract: Reverse osmosis (RO) is the most widely used technology to desalinate brackish water and seawater. Significant efforts have been made in recent decades to improve RO efficiency. Feed spacer geometry design is a very important factor in RO membrane performance. In this work, correlations based on computational fluid dynamics and experimental work were applied in an algorithm to simulate the effect of different feed spacer geometries in full-scale brackish water reverse osmosis (BWRO) membranes with different permeability coefficients. The aim of this work was to evaluate the impact of feed spacers in conjunction with the permeability coefficients on membrane performance. The results showed a greater impact of feed spacer geometries in the membrane with the highest water permeability coefficient (A). Studying only one single element in a series, variations due to feed spacer geometries were observed in specific energy consumption (SEC) and permeate concentration (C_p) of about 6.83% and 10.42%, respectively. Allowing the rolling of commercial membranes with different feed spacer geometries depending on the operating conditions could optimize the RO process.

Keywords: reverse osmosis; feed spacers; spiral-wound membrane modules; membrane performance

1. Introduction

Reverse osmosis (RO) technology is the most extensively used technology for the desalination of both seawater and brackish water [1,2]. Among the current desalination technologies used in full-scale plants, RO is the most energy-efficient one [1]. Nonetheless, RO is an intensive energy consumption process [3,4]. One of the main challenges to improve RO efficiency is related to decreasing specific energy consumption (SEC) [5,6] and the fouling effects on spiral-wound membrane modules (SWMMs) of RO. In recent years, several studies have proposed alternatives to improve the efficiency of the process, such as using new membrane materials [7–9] and optimizing the feed spacer geometry [10,11]. Generally, the studies related to new RO membrane materials have focused on improving certain membrane characteristics, namely their antifouling properties [12,13], the water permeability coefficient (A), and the solute permeability coefficient (B) [14]. However, the feed spacers are an essential part of SWMMs and play an important role in the concentration polarization phenomena, the pressure drop along the membrane, and fouling [10,15,16].

Research on feed spacer design has shown the impact of feed spacer geometry on feed channel hydrodynamics, which in turn affect other parameters. Many studies have been made on feed spacer geometry. In 1987, Schock and Miquel [17] experimentally developed correlations for the friction factor (λ) and Sherwood number (Sh) for SWMMs of RO membranes. λ depends on the Reynolds number (Re) and on two parameters, and Sh depends on Re, the Schmidt number (Sc), and three parameters.

Sh is related to the mass transfer coefficient (*k*) and the polarization factor (*PF*). V. Geraldes et al. [18] modified the correlation of λ by adding an additional factor (K_λ) to take into consideration pressure losses in the feed of the pressure vessels (PVs) and SWMM fittings. In their work, these correlations were used to simulate and optimize medium-sized seawater reverse osmosis (SWRO) processes. Abbas [19] used a different correlation for λ obtained in a previous work [20] for ultrafiltration (UF) membranes. This correlation depends on *Re* and three parameters and was used to simulate an industrial water desalination plant. In 2004, Schwinge et al. [21] used the correlation for UF membranes but removing one parameter. The fouling effect in SWMMs was studied using computational fluid dynamics (CFD) in the aforementioned work. These previous studies do not allow consideration to be given to different feed spacer geometries, which have different λ and *Sh*. Koutsou et al. [22] went a step further by proposing different correlations for the dimensionless pressure drop (proportional to the friction factor), taking into account the ratio of the distance between parallel filaments and the filament diameter (L/d), the angle between the crossing filaments (β), and the flow attack angle (α). In that work, a new equation to determine a dimensionless pressure drop was formulated. In a later study, Koutsou et al. [23] used the same correlations of Schock and Miquel to estimate the *Sh* for different feed spacer geometries. These correlations are applicable to simulations of full-scale systems as long computation times are not required, as happens with the CFD. Guillen and Hoek [24] considered the pressure drop, concentration polarization, and the shape of the filament in a performance study of the RO process. The study was carried out proposing a three parameters dependent correlation for λ and the typical correlation for the *Sh*. Different geometries of the mesh were not considered in the study. Haidari et al. [25] evaluated the performance of six commercial feed spacers in terms of pressure drop. The effect of the concentration polarization and membrane characteristics were not taken in account in that study.

A study of the different feed spacer geometries in a full-scale commercial RO SWMM required equations that can be applied without the computation requirements of CFD (Navier–Stokes equations). This is the reason simple correlations such as those proposed by Schock and Miquel [17] or Koutsou et al. [22,23] are needed. Another important factor that needs to be taken into consideration concerns the permeability coefficients *A* and *B* of the membranes. Different values of these coefficients can play an important role in the optimization of feed spacer geometries. This paper provides simulations and a performance analysis for different permeability coefficients, feed spacer geometries for brackish water RO SWMMs, and feed concentrations (C_f).

2. Methodology

In this study, three RO SWMMs for BW were considered, FILMTEC[TM] BW30-400, FILMTEC[TM] ECO PRO-400, and FILMTEC[TM] FORTLIFE[TM] CR100 PRO-400 from Dow[®] company (Midland, MI, USA). The Water Application Value Engine (WAVE) software from the same company was used to calculate the permeability coefficients *A* and *B* of the membranes. Table 1 shows the calculated permeability coefficients.

Table 1. Calculated permeability coefficients.

Membrane	A (m Pa s^{-1})	B (m s^{-1})
FILMTEC[TM] BW30-400	9.63×10^{-12}	5.58×10^{-8}
FILMTEC[TM] ECO PRO-400	1.60×10^{-11}	4.24×10^{-8}
FILMTEC[TM] FORTLIFE[TM] CR100 PRO-400	1.06×10^{-11}	4.16×10^{-8}

In order to compare the three full scale BWRO membranes, the PVs of one element were simulated. A range between 1 and 15 g L^{-1} as C_f of NaCl was used with feed flow (Q_f) and feed pressure (p_f) ranges from 3 to 17 m^3 h^{-1} and from 1 to 42 bar, respectively. The different feed spacer geometries studied by Koutsou et al. [22] were considered. The performance of these three membranes wound

with different feed spacer geometries was simulated. Solution–diffusion [26,27], which assumes that the membrane is nonporous (without imperfections), was the method of transport used. The theory is that transport through the membrane occurs as the molecule of interest dissolves in the membrane and then diffuses through the membrane. This holds true for both the solvent and solute in solution. In this model, the solvent and solute transport are independent of each other (Equations (1) and (2)). This is the most widely accepted model and provides results close to the real behavior of these systems. The transport equations use mean values of membrane elements, and pressure drop in the permeate as well as temperature changes along the RO system are disregarded.

The transport equations used were the following:

$$Q_{\mathrm{p}} = A \times (\Delta p - \Delta \pi) \times S_{\mathrm{m}}, \tag{1}$$

where Q_{p} is the permeate flow, A is the membrane permeability coefficient, $(\Delta p - \Delta \pi)$ is the net driven pressure (NDP), and S_{m} is the membrane area.

Solute transport equation:

$$Q_{\mathrm{s}} = B \times \Delta C \times S_{\mathrm{m}}, \tag{2}$$

where Q_{s} is the solute flow through the membrane, B is the solute permeability coefficient of the membrane, and ΔC is the concentration gradient of solute on either side of the membrane.

Coefficient A (Equation (1)) usually depends on three variables: Average osmotic pressure on the membrane surface (π_{m}), temperature, and flow factor related to fouling and operating time (FF) [28]. FF is an important parameter below 1 that represents the decrease of the coefficient A due to fouling [29]. There are several methods that try to predict this parameter [30]. As this work is about a comparison between different feed spacer geometries used in three different membranes based on simulations, it was considered that the fouling factor FF was 1 (new membrane). Usually, the FF decreases with the operating time as SWMMs get fouled [29]. Feed temperature was considered 25 °C, so the temperature correction factor (TCF) is equal to 1 and the effect of osmotic pressure on A was neglected.

$$A = A(A_0, \pi_{\mathrm{m}}) \times TCF \times FF, \tag{3}$$

where A_0 is the initial water permeability coefficient. Next in the development of Equation (1) is the expression of the NDP, which depends on p_{f}, pressure drop (Δp_{fb}), permeate pressure (p_{p}), π_{m}, and average osmotic pressure of the permeate (π_{p}):

$$NDP = (\Delta p - \Delta \pi) = p_{\mathrm{f}} - \frac{\Delta p_{\mathrm{fb}}}{2} - p_{\mathrm{p}} - \pi_{\mathrm{m}} + \pi_{\mathrm{p}}. \tag{4}$$

Δp_{fb} was calculated as follows [31]:

$$\Delta p_{\mathrm{fb}} = \lambda \times L \times \frac{\rho}{d_{\mathrm{h}}} \frac{v_{\mathrm{fb}}}{2}, \tag{5}$$

$$d_{\mathrm{h}} = \frac{4\epsilon}{\frac{2}{h} + (1 - \epsilon)\frac{8}{h}}, \tag{6}$$

where L is the SWMM length (it was considered 1 m), ρ is the average feed-brine density ($\sim 1000\ \mathrm{kg\,m}^{-3}$ for BW), v_{fb} is the average feed-brine water velocity ($\mathrm{m\,s}^{-1}$), d_{h} (m) is the hydraulic diameter of the feed channel, ϵ is the porosity of the cross section area in the feed channel (0.89 [17]), and h is the height of the feed channel, which was considered 28 mili inches (7.11×10^{-4} m) for the three membranes. In this study, the pressure losses in the permeate channel were not considered; a value of $p_{\mathrm{p}} = 5$ psi (34,473.8 Pa) was used. Figure 1 shows the different parameters of feed spacer geometries. The correlations used for λ were proposed by Koutsou et al. [22] (Table 2). λ was multiplied by the parameter K_λ, which was introduced by Geraldes et al. [18]. This factor takes into consideration

additional pressure losses in the feed of the PVs and module fittings. Values between 1.9 and 2.9 were obtained in that study. A value of 2.5 was used in this paper.
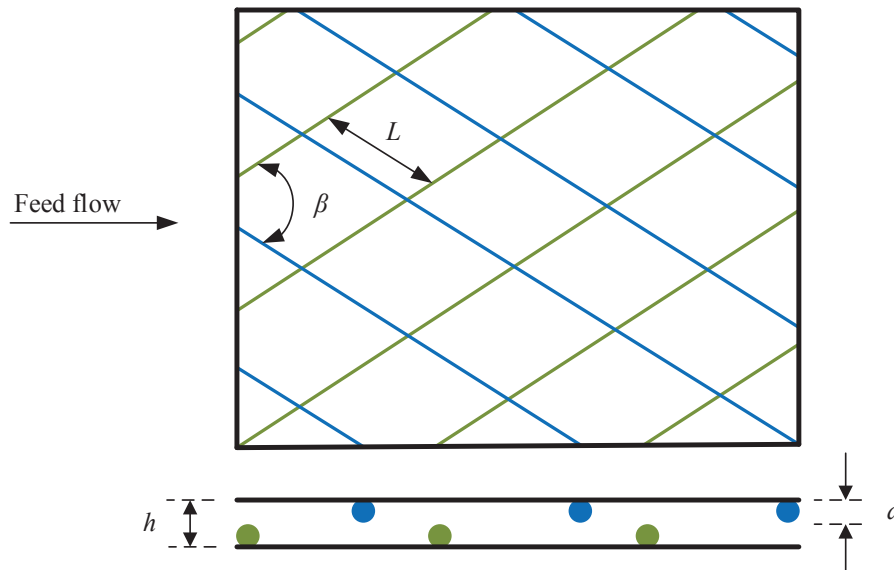

Figure 1. Parameters of feed spacer geometries.

Table 2. Correlation between λ and Re number [22].

	$\beta = 90°$	$\beta = 105°$	$\beta = 120°$
$L/d = 6$	$2.3Re^{-0.31}$	$2.2Re^{-0.23}$	$3.8Re^{-0.18}$
$L/d = 8$	$0.8Re^{-0.19}$	$0.9Re^{-0.15}$	$1.2Re^{-0.14}$
$L/d = 12$	$1.5Re^{-0.40}$	$1.1Re^{-0.31}$	$0.7Re^{-0.19}$

As water flows across the membrane, the rejected solute can accumulate on the membrane surface where the solute concentration will increase. This concentration generates a diffusive flow back to the feed flow. Steady state conditions are established after a certain period of time in steady conditions. PF provides the relationship between C_m and C_f. In order to calculate π_p, the average ionic permeability coefficient (B) was used (Equation (7)). This enables a calculation of the ion concentration of the permeate (C_p):

$$C_p = B \times PF \times TCF \times \frac{S_m}{Q_p} \times \left(\frac{C_f \times (1 + CF)}{2} \right), \tag{7}$$

$$\pi_m = \pi_f \times \frac{C_{fb}}{C_f} \times PF, \tag{8}$$

where CF is the concentration factor, π_f is the osmotic pressure of feedwater, and C_{fb} is the average feed-brine solute concentration.

$$\pi_f = 0.0787 \times (273 + T) \times \Sigma m, \tag{9}$$

$$C_m = C_{fb} \times PF, \tag{10}$$

$$PF = \frac{C_m}{C_a} = e^{\frac{J}{k}}, \tag{11}$$

where m is the molal concentration of NaCl, C_m in the concentration of solute on the membrane surface, J is the permeate flux per unit area, and k is the mass transfer coefficient, which is given by Sh [17]:

$$Sh = \frac{k \times d_\mathrm{h}}{D} = a \times Re^b \times Sc^c, \tag{12}$$

$$Re = \frac{\rho \times v_\mathrm{fb} \times d_\mathrm{h}}{\eta}, \tag{13}$$

$$Sc = \frac{\eta}{\rho \times D}, \tag{14}$$

where a, b and c are parameters, Sc is the Schmidt number, ρ ($\mathrm{kg\,m^{-3}}$) is the water density, v_fb is the feed-brine velocity ($\mathrm{m\,s^{-1}}$), and η (0.000891 $\mathrm{kg\,m^{-1}\,s^{-1}}$ for T = 25 °C) the dynamic viscosity. Koutsou et al. [23] calculated correlations for the Sh for different feed spacer geometries (Table 3). The solute diffusivity (D ($\mathrm{m^2\,s^{-1}}$)) was calculated as follows [32]:

$$D = \left(0.72598 + 0.023087T + 0.00027657T^2\right) \times 10^{-9}. \tag{15}$$
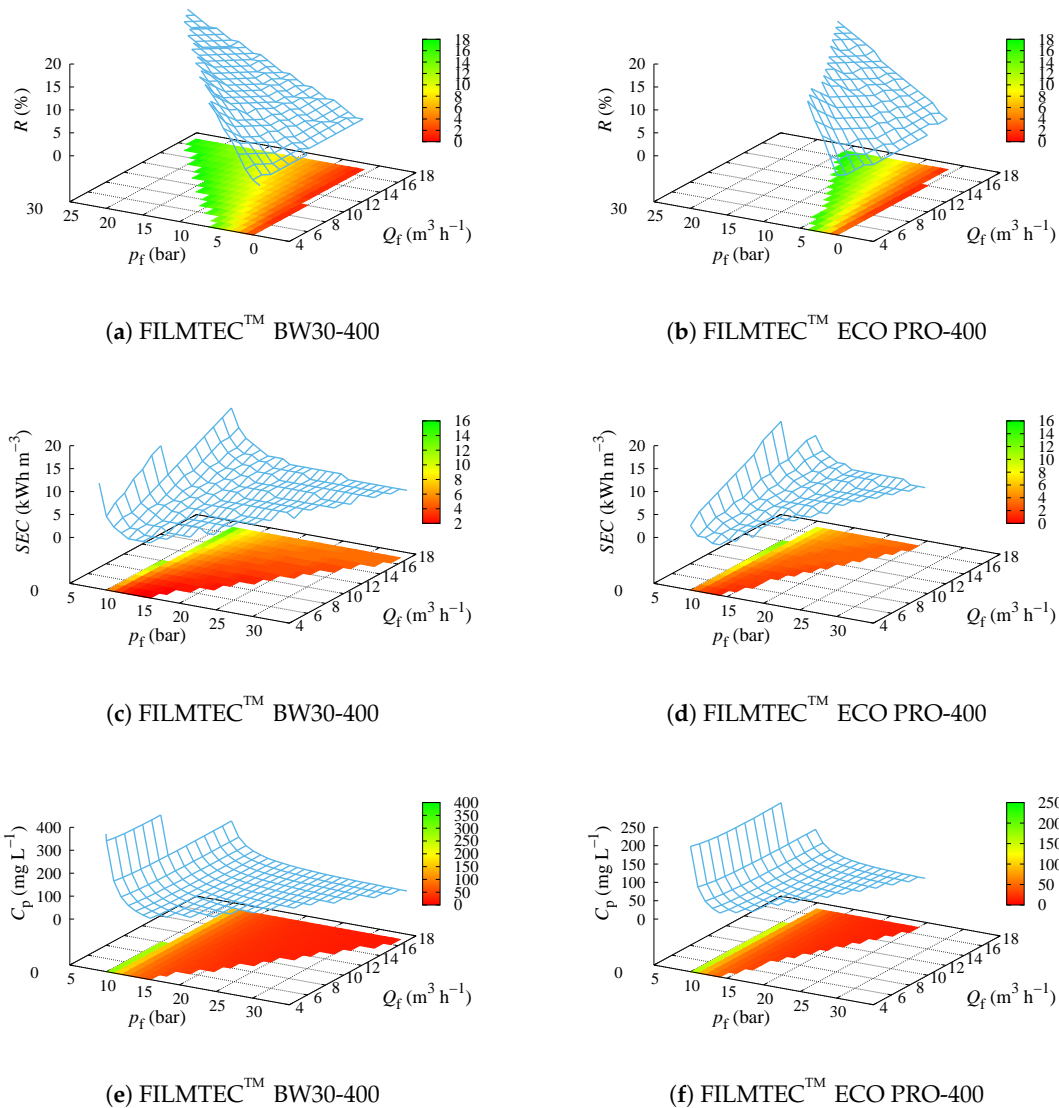
Table 3. Sh as function of Re and Sc for different feed spacer geometries [23].

	$\beta = 90°$	$\beta = 105°$	$\beta = 120°$
$L/d = 6$	$0.14Re^{0.64}Sc^{0.42}$	$0.08Re^{0.715}Sc^{0.48}$	$0.073Re^{0.87}Sc^{0.45}$
$L/d = 8$	$0.16Re^{0.605}Sc^{0.42}$	$0.17Re^{0.625}Sc^{0.42}$	$0.12Re^{0.71}Sc^{0.43}$
$L/d = 12$	$0.26Re^{0.57}Sc^{0.37}$	$0.17Re^{0.64}Sc^{0.40}$	$0.19Re^{0.645}Sc^{0.38}$

In order to calculate all the above variables, an algorithm already proposed by the authors was used [33] and implemented in MATLAB® (MathWorks, Natick, MA, USA). To calculate the SEC, a performance of 80% of the high pressure pump was assumed. SEC was determined with the feed pressure, feed flow, water density, and the abovementioned performance of the high pressure pump and dividing by permeate flow. The results that exceeded the operating limits established by the manufacturer were discarded (minimum concentrate flow of 3 $\mathrm{m^3\,h^{-1}}$, 19% as maximum element recovery, etc.).

3. Results and Discussion

Figure 2 shows the flux recovery (R), SEC, and C_p of the FILMTEC™ BW30-400 and FILMTEC™ ECO PRO-400 membranes, with a a C_f = 5 g $\mathrm{L^{-1}}$, L/d = 6 and β = 90°. FILMTEC™ ECO PRO-400 membrane has a higher A than FILMTEC™ BW30-400 (Table 1). Consequently, high R values are reached with lower p_f than with FILMTEC™ BW30-400, but the operating range is wider for the BW30 than for the ECO PRO (Figure 2a,b). The reason is that the ECO PRO membrane produces so much water that as the pressure rises, the concentrate flowrate decreases considerably, reaching the minimum established by the manufacturer with not very high pressures. This factor must be taken into account when this type of membrane is placed in series. Figure 2c,d shows that low SEC were reached with Q_f values ranging between 4 and 10 $\mathrm{m^3\,h^{-1}}$. This range varies if various SWMMs are arranged in series. The C_p decreased with increasing Q_f and p_f due to B being constant, and the higher the v_fb, the lower the PF and C_m. It should be noted that variations of C_f and/or of the permeability coefficients (due to fouling) could significantly change the values of the operating points.

(**a**) FILMTEC™ BW30-400

(**b**) FILMTEC™ ECO PRO-400

(**c**) FILMTEC™ BW30-400

(**d**) FILMTEC™ ECO PRO-400

(**e**) FILMTEC™ BW30-400

(**f**) FILMTEC™ ECO PRO-400

Figure 2. *R*, *SEC*, and C_P of two studied membranes with different permeability coefficients, C_f = 5 g L^{-1}, L/d = 6 and β = 90°. (**a,c,e**) FILMTEC™ BW30-400; (**b,d,f**) FILMTEC™ ECO PRO-400.

Figures 3 and 4 show the exponential growth of *SEC* with the increase of C_f. As C_f increases. there is a slight increase in the separation of the exponential curves of each feed spacer geometry. This reveals that the effect of the feed spacer geometry on *SEC* in seawater desalination is more pronounced than in brackish water. The *SEC* was lower for the membrane with the higher coefficient *A*, but the separation between curves was higher for the ECO PRO membrane than for the BW30-400. This shows that the impact of the feed spacer geometry with the C_f was higher for the FILMTEC™ ECO PRO-400 membrane.
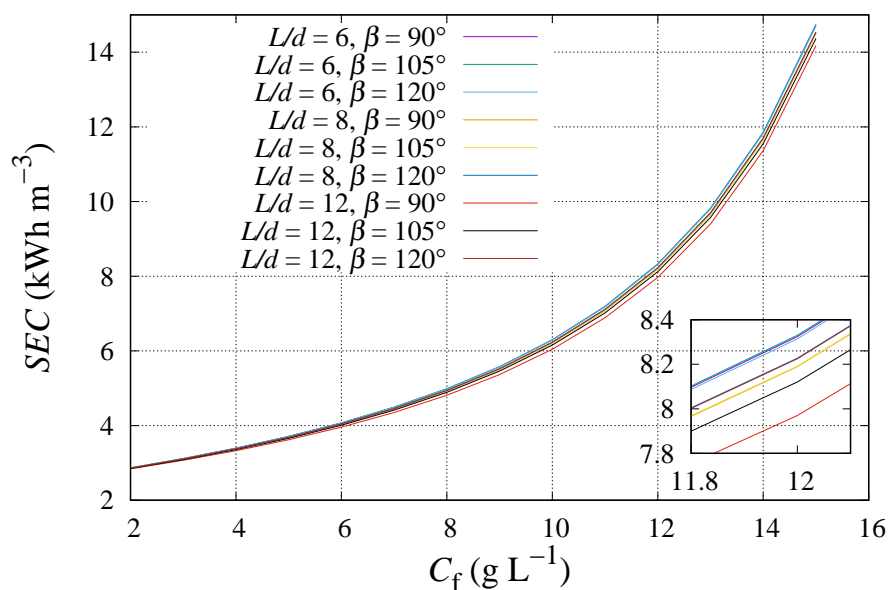
Figure 3. *SEC* of the membrane FILMTEC™ BW30-400 considering different feed spacer geometries, a range of C_f, $p_f = 15$ bar and $Q_f = 11$ m³ h⁻¹.
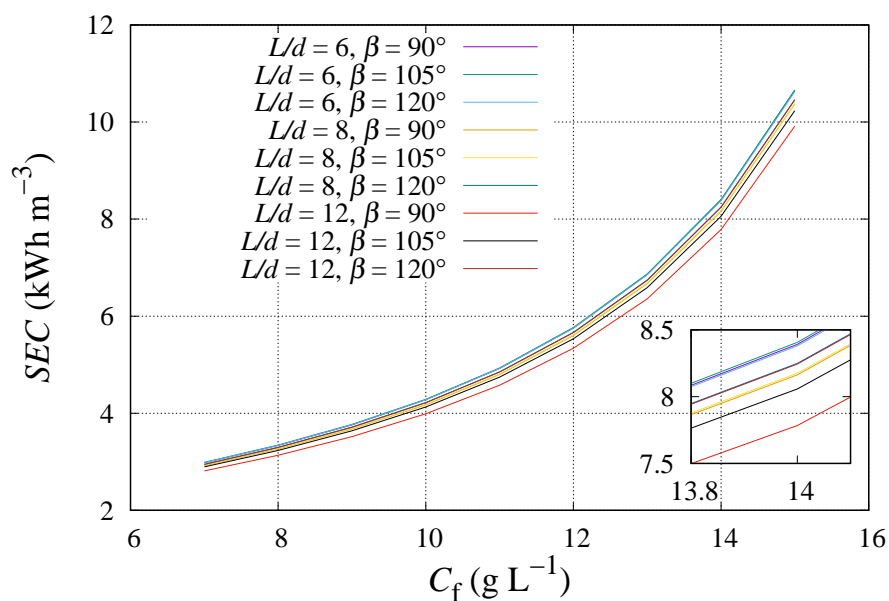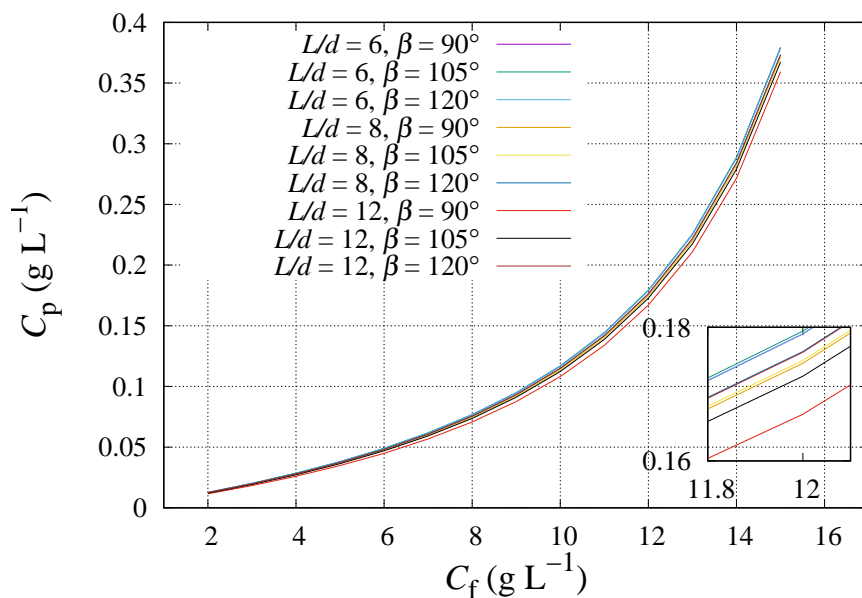

Figure 4. *SEC* of the membrane FILMTEC™ ECO PRO-400 considering different feed spacer geometries, a range of C_f, $p_f = 15$ bar and $Q_f = 11$ m³ h⁻¹.

As happened with *SEC*, C_p also showed an exponential growth with the increase of C_f for both membranes (Figures 5 and 6). Again, bigger differences between curves were reached at higher C_f values and were even more pronounced for the membrane with the highest coefficient *A*. The membrane with the lowest coefficient *B* has the lowest C_p as was expected.

The studied was carried out considering four different feedwater conditions, where the average *R* were, for the cases 1 and 2, 8.63, 13.59, and 9.41% for the membranes FILMTEC™ BW30-400, FILMTEC™ ECO PRO-400, and FILMTEC™ FORTLIFE™ CR100 PRO-400, respectively. For the cases 3 and 4, in the same order of membranes, the average *R* were 9.11, 13.74, and 9.86%. Table 4 shows the *SEC* results for the three different membrane studied, considering different feed spacer geometries.

In case 1, the *SEC* variations were 1.23, 3.17, and 1.55%. The membrane with the highest *A* was more influenced by the feed spacer geometry in terms of *SEC*. The second case is similar to the first one, but Q_f was reduced from 12 to 8 m^3 h^{-1}. In this case, Table 4 only shows results for the FILMTEC^{TM} BW30-400 and FILMTEC^{TM} FORTLIFE^{TM} CR100 PRO-400 membranes, as the results obtained for the FILMTEC^{TM} ECO PRO-400 were outside the recommended range of the manufacturer. The variations were higher than in the previous case, namely 2.42 and 2.74%, respectively. The *SEC* values were lower in the second case, as pressure losses decreased as a consequence of the reduction of the velocity in the feed channel. For the next cases (3 and 4), C_f increased from 5 to 10 g L^{-1} and p_f from 13 to 18 bar. The results of case 3 showed higher *SEC* values and variations of 3.7, 6.83, and 4.19%. The higher the C_f, the more pronounced the *SEC* variations, because the highe the C_f was, the higher the concentration polarization effect was on membrane performance and the role played by spacer geometries was more pronounced in terms of membrane production. These phenomena can be appreciated in Figures 3 and 4: The higher the C_f, the more separated the curves are. The decrease of Q_f to 8 m^3 h^{-1} had a pronounced impact on the *SEC* variation. The variations in the third case were 4.95 and 5.46% for the FILMTEC^{TM} BW30-400 and FILMTEC^{TM} FORTLIFE^{TM} CR100 PRO-400 membranes, respectively. Variation of the FILMTEC^{TM} ECO PRO-400 membrane was 2.95%, but the results for two feed spacer geometries were not considered, as they were outside the recommended range. The *SEC* was affected by feed spacer geometry because it also affected the pressure drop along the membrane and the *PF*. The higher the pressure losses are, the lower the permeate production is, and the higher the concentration polarization (polarization factor) is, the higher the osmotic pressure on the membrane surface and the lower the permeate production. The lowest *SEC* for each membrane corresponded with the same feed spacer geometry ($L/d = 6$ and $\beta = 120°$). The membranes reached the highest *SEC* with $L/d = 8$ and $\beta = 90°$, except the FILMTEC^{TM} BW30-400 and FILMTEC^{TM} FORTLIFE^{TM} CR100 PRO-400 membranes in case 1, where the highest *SEC* was reached with $L/d = 6$ and $\beta = 90°$.

Figure 5. C_p of the membrane FILMTEC^{TM} BW30-400 considering different feed spacer geometries, a range of C_f, p_f = 15 bar and Q_f = 11 m^3 h^{-1}.
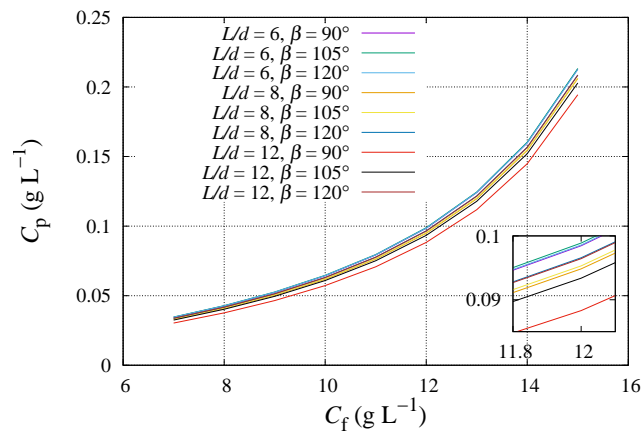
Figure 6. C_p of the membrane FILMTEC$^{\text{TM}}$ ECO PRO-400 considering different feed spacer geometries, a range of C_f, $p_f = 15$ bar and $Q_f = 11$ m^3 h^{-1}.

Table 4. *SEC* (kWh m^{-3}) for the three membranes studied with different spacer geometries.

Inputs	L/d	β	BW30-400	ECO PRO-400	FORTLIFE
$C_f = 5\ p_f = 13\ Q_f = 12$ (case 1)	6	90°	5.1617	3.2923	4.7354
		105°	5.1288	3.2501	4.6984
		120°	5.0984	3.1908	4.6622
	8	90°	5.1606	3.2954	4.7329
		105°	5.1257	3.2542	4.6969
		120°	5.1065	3.2304	4.6787
	12	90°	5.1555	3.2927	4.7290
		105°	5.1283	3.2633	4.7024
		120°	5.1284	3.2625	4.7023
$C_f = 5\ p_f = 13\ Q_f = 8$ (case 2)	6	90°	3.5373	-	3.2560
		105°	3.5051	-	3.2230
		120°	3.4523	-	3.1675
	8	90°	3.5379	-	3.2569
		105°	3.5041	-	3.2225
		120°	3.4891	-	3.2068
	12	90°	3.5329	-	3.2524
		105°	3.5153	-	3.2346
		120°	3.5145	-	3.2338
$C_f = 10\ p_f = 18\ Q_f = 12$ (case 3)	6	90°	6.8082	4.5469	6.2941
		105°	6.7110	4.4351	6.1922
		120°	6.5656	4.2523	6.0408
	8	90°	6.8175	4.5638	6.3049
		105°	6.7236	4.4583	6.2101
		120°	6.6688	4.3935	6.1523
	12	90°	6.8118	4.5601	6.2996
		105°	6.7475	4.4887	6.2328
		120°	6.7452	4.4851	6.2304
$C_f = 10\ p_f = 18\ Q_f = 8$ (case 4)	6	90°	4.7850	3.3178	4.4495
		105°	4.7044	3.2282	4.3669
		120°	4.5547	-	4.2134
	8	90°	4.7916	3.3263	4.4570
		105°	4.7081	3.2350	4.3717
		120°	4.6676	-	4.3311
	12	90°	4.7811	3.3157	4.4465
		105°	4.7391	3.2706	4.4040
		120°	4.7367	3.2679	4.4018

Table 5 shows the results obtained for C_p in the same four cases. In general, the impacts of the feed spacer geometries were higher for C_p than for SEC. In the first case, the C_p had variations of 6.18, 10.42, and 6.86%, respectively. The FILMTEC[TM] ECO PRO-400 membrane had higher variations than the other membranes due to the coefficient A, so the velocity in the feed channel also had higher variations for the FILMTEC[TM] ECO PRO-400 membrane than others, which makes the impact of feed spacer geometries more pronounced for the mentioned membrane. In the salt rejection, the coefficient B plays an important role, but so too does coefficient A. The coefficients B of the FILMTEC[TM] ECO PRO-400 and FILMTEC[TM] FORTLIFE[TM] CR100 PRO-400 membranes are very similar, though slightly higher for the FILMTEC[TM] ECO PRO-400 membrane. However, the values of C_p were higher for the FILMTEC[TM] FORTLIFE[TM] CR100 PRO-400 membrane due to R. The FILMTEC[TM] ECO PRO-400 membrane showed a 4% higher recovery than the other two, which resulted in a decrease of C_p despite the increase of C_m. The lowest values of C_p were reached with $L/d = 6$ and $\beta = 120°$ for the three membranes. The highest values corresponded to $L/d = 8$, $L/d = 12$, and $\beta = 90°$, depending on the case.

Table 5. C_p (g L^{-1}) for the three membranes studied with different spacer geometries.

Inputs	L/d	β	BW30-400	ECO PRO-400	FORTLIFE
	6	90°	0.0421	0.0224	0.0292
		105°	0.0412	0.0215	0.0285
		120°	0.0397	0.0202	0.0273
$C_f = 5$ $p_f = 13$ $Q_f = 12$ (case 1)	8	90°	0.0423	0.0225	0.0293
		105°	0.0414	0.0217	0.0286
		120°	0.0408	0.0213	0.0282
	12	90°	0.0422	0.0225	0.0293
		105°	0.0416	0.0220	0.0288
		120°	0.0416	0.0220	0.0288
	6	90°	0.0456	-	0.0319
		105°	0.0445	-	0.0310
		120°	0.0423	-	0.0294
$C_f = 5$ $p_f = 13$ $Q_f = 8$ (case 2)	8	90°	0.0458	-	0.0320
		105°	0.0446	-	0.0311
		120°	0.0440	-	0.0307
	12	90°	0.0456	-	0.0319
		105°	0.0450	-	0.0315
		120°	0.0450	-	0.0314
	6	90°	0.0809	0.0446	0.0565
		105°	0.0785	0.0426	0.0547
		120°	0.0744	0.0391	0.0515
$C_f = 10$ $p_f = 18$ $Q_f = 12$ (case 3)	8	90°	0.0813	0.0450	0.0568
		105°	0.0790	0.0431	0.0551
		120°	0.0776	0.0419	0.0540
	12	90°	0.0813	0.0450	0.0568
		105°	0.0797	0.0437	0.0556
		120°	0.0796	0.0437	0.0556
	6	90°	0.0896	0.0522	0.0632
		105°	0.0867	0.0499	0.0610
		120°	0.0812	-	0.0568
$C_f = 10$ $p_f = 18$ $Q_f = 8$ (case 4)	8	90°	0.0899	0.0525	0.0634
		105°	0.0870	0.0501	0.0612
		120°	0.0856	-	0.0601
	12	90°	0.0896	0.0522	0.0632
		105°	0.0882	0.0511	0.0621
		120°	0.0881	0.0510	0.0620

It should be noted that the simulations were carried out considering only one SWMM in the PV. These small variations in terms of *SEC* and C_p could be increased by studying more SWMMs in a series. Full-scale BWRO desalination plants usually have two stages with 5 or more SWMMs in a series per stage and even variations in the C_f.

4. Conclusions

This study has shown the impact of feed spacer geometries on *SEC* and C_p in full-scale SWMMs for BWRO desalination. The results showed that the optimal feed spacer geometry depends on operating conditions and permeability coefficients. The variations of *SEC* and C_p were not so high for each membrane considering different spacer geometries, but these differences could be more pronounced if six BWRO SWMMs are arranged in a series, as is often the case. The membrane with the highest coefficient *A* showed higher variations with different feed spacer geometries than the others. Manufacturers should consider not only the permeability coefficients *A* and *B*, but also different feed spacer configurations for the same membrane. The possibility of having the same membrane with different feed spacers could be used to optimize the RO process. Usually, membrane manufacturers offer membranes with different permeability coefficients, active area or feed spacer thickness, but with an established feed spacer geometry. Manufacturer software allows the simulation of different membrane elements in the same PV, but without considering different feed spacer geometries.

This work is based on simulations using experimental work in flat sheet configurations. Experimental work using different SWMMs rolled with different feed spacers should be carried out to have more consistent experimental support. A study of the long-term fouling effect is also desirable to have a deeper knowledge about the role of feed spacers in full-scale BWRO desalination plants.

Author Contributions: Formal analysis, A.R.-G.; Funding acquisition, A.R.-G.; Investigation, A.R.-G.; Software, A.R.-G.; Supervision, I.N.P.; Visualization, A.R.-G.; Writing—original draft, A.R.-G.; Writing—review and editing, A.R.-G. and I.N.P.

Conflicts of Interest: The authors declare no conflict of interest.

Nomenclature

Acronyms

PV	Pressure vessel
RO	Reverse osmosis
A	Water permeability coefficient (m day^{-1} kg^{-1} cm^2)
B	Ion permeability coefficient (m day^{-1})
C	Concentration (mg L^{-1})
D	Solute diffusivity (m^2 s^{-1})
d	Filament diameter (m)
d_h	Hydraulic diameter (m)
FF	Flow factor
J	Flow per unit area (m^3 m^{-2} day^{-1})
K_λ	Additional pressure losses factor
k	Mass transfer coefficient
L	Cylinder spacing (m)
m	Molal concentration (mol kg^{-1})
NDP	Net driven pressure (kg cm^{-2})
P	Solute pass (%)
PF	Polarization factor
PV	Pressure vessel
p	Pressure (kg cm^{-2})
Q	Flow (m^3 day^{-1})
R	Flow recovery (%)

Re	Reynolds number
RO	Reverse osmosis
S_m	Membrane surface (m^2)
Sc	Schmidt number
SEC	Specific energy consumption ($kW\,h\,m^{-3}$)
Sh	Sherwood number
TCF	Temperature correction factor
Y	Fraction recovery
Greek letters	
β	Angle between crossing filaments
η	Dynamic viscosity ($kg\,m^{-1}\,s$)
λ	Friction factor
ν	Velocity ($m\,s^{-1}$)
π	Osmotic pressure ($kg\,cm^{-2}$)
ρ	Density ($kg\,m^{-3}$)
Δp	Pressure gradient ($kg\,cm^{-2}$)
$\Delta\pi$	Osmotic pressure gradient ($kg\,cm^{-2}$)
ΔC	Concentration gradient ($mg\,L^{-1}$)
Subscripts	
av	Average
f	Feed
m	Membrane
p	Permeate
b	Brine
s	Solute

References

1. Miller, S.; Shemer, H.; Semiat, R. Energy and environmental issues in desalination. *Desalination* **2015**, *366*, 2–8. [CrossRef]
2. Gao, L.; Yoshikawa, S.; Iseri, Y.; Fujimori, S.; Kanae, S. An Economic Assessment of the Global Potential for Seawater Desalination to 2050. *Water* **2017**, *9*, 763. [CrossRef]
3. Shemer, H.; Semiat, R. Sustainable RO desalination—Energy demand and environmental impact. *Desalination* **2017**, *424*, 10–16. [CrossRef]
4. Stillwell, A.S.; Webber, M.E. Predicting the Specific Energy Consumption of Reverse Osmosis Desalination. *Water* **2016**, *8*, 601. [CrossRef]
5. Kurihara, M.; Takeuchi, H. SWRO-PRO System in "Mega-ton Water System" for Energy Reduction and Low Environmental Impact. *Water* **2018**, *10*, 48. [CrossRef]
6. Park, H.G.; Kwon, Y.N. Long-Term Stability of Low-Pressure Reverse Osmosis (RO) Membrane Operation—A Pilot Scale Study. *Water* **2018**, *10*, 93. [CrossRef]
7. Goh, P.; Matsuura, T.; Ismail, A.; Hilal, N. Recent trends in membranes and membrane processes for desalination. *Desalination* **2016**, *391*, 43–60. [CrossRef]
8. Ismail, A.; Padaki, M.; Hilal, N.; Matsuura, T.; Lau, W. Thin film composite membrane—Recent development and future potential. *Desalination* **2015**, *356*, 140–148. [CrossRef]
9. Aani, S.A.; Haroutounian, A.; Wright, C.J.; Hilal, N. Thin Film Nanocomposite (TFN) membranes modified with polydopamine coated metals/carbon-nanostructures for desalination applications. *Desalination* **2018**, *427*, 60–74. [CrossRef]
10. Haidari, A.; Heijman, S.; van der Meer, W. Optimal design of spacers in reverse osmosis. *Separ. Purif. Technol.* **2018**, *192*, 441–456. [CrossRef]
11. Kavianipour, O.; Ingram, G.D.; Vuthaluru, H.B. Investigation into the effectiveness of feed spacer configurations for reverse osmosis membrane modules using Computational Fluid Dynamics. *J. Membr. Sci.* **2017**, *526*, 156–171. [CrossRef]

12. Dong, C.; Wang, Z.; Wu, J.; Wang, Y.; Wang, J.; Wang, S. A green strategy to immobilize silver nanoparticles onto reverse osmosis membrane for enhanced anti-biofouling property. *Desalination* **2017**, *401*, 32–41. [CrossRef]

13. Saeki, D.; Tanimoto, T.; Matsuyama, H. Anti-biofouling of polyamide reverse osmosis membranes using phosphorylcholine polymer grafted by surface-initiated atom transfer radical polymerization. *Desalination* **2014**, *350*, 21–27. [CrossRef]

14. Werber, J.R.; Deshmukh, A.; Elimelech, M. The Critical Need for Increased Selectivity, Not Increased Water Permeability, for Desalination Membranes. *Environ. Sci. Technol. Lett.* **2016**, *3*, 112–120. [CrossRef]

15. Abid, H.S.; Johnson, D.J.; Hashaikeh, R.; Hilal, N. A review of efforts to reduce membrane fouling by control of feed spacer characteristics. *Desalination* **2017**, *420*, 384–402. [CrossRef]

16. Xie, P.; Murdoch, L.C.; Ladner, D.A. Hydrodynamics of sinusoidal spacers for improved reverse osmosis performance. *J. Membr. Sci.* **2014**, *453*, 92–99. [CrossRef]

17. Schock, G.; Miquel, A. Mass transfer and pressure loss in spiral wound modules. *Desalination* **1987**, *64*, 339–352. [CrossRef]

18. Geraldes, V.; Pereira, N.E.; de Pinho, M.N. Simulation and Optimization of Medium-Sized Seawater Reverse Osmosis Processes with Spiral-Wound Modules. *Ind. Eng. Chem. Res.* **2005**, *44*, 1897–1905. [CrossRef]

19. Abbas, A. Simulation and analysis of an industrial water desalination plant. *Chem. Eng. Process.* **2005**, *44*, 999–1004. [CrossRef]

20. Costa, A.D.; Fane, A.; Wiley, D. Spacer characterization and pressure drop modelling in spacer-filled channels for ultrafiltration. *J. Membr. Sci.* **1994**, *87*, 79–98. [CrossRef]

21. Schwinge, J.; Neal, P.; Wiley, D.; Fletcher, D.; Fane, A. Spiral wound modules and spacers: Review and analysis. *J. Membr. Sci.* **2004**, *242*, 129–153. [CrossRef]

22. Koutsou, C.; Yiantsios, S.; Karabelas, A. Direct numerical simulation of flow in spacer-filled channels: Effect of spacer geometrical characteristics. *J. Membr. Sci.* **2007**, *291*, 53–69. [CrossRef]

23. Koutsou, C.; Yiantsios, S.; Karabelas, A. A numerical and experimental study of mass transfer in spacer-filled channels: Effects of spacer geometrical characteristics and Schmidt number. *J. Membr. Sci.* **2009**, *326*, 234–251. [CrossRef]

24. Guillen, G.; Hoek, E.M. Modeling the impacts of feed spacer geometry on reverse osmosis and nanofiltration processes. *Chem. Eng. J.* **2009**, *149*, 221–231. [CrossRef]

25. Haidari, A.; Heijman, S.; van der Meer, W. Effect of spacer configuration on hydraulic conditions using PIV. *Separ. Purif. Technol.* **2018**, *199*, 9–19. [CrossRef]

26. Wijmans, J.; Baker, R. The solution-diffusion model: A review. *J. Membr. Sci.* **1995**, *107*, 1–21. [CrossRef]

27. Al-Obaidi, M.; Kara-Zaitri, C.; Mujtaba, I. Scope and limitations of the irreversible thermodynamics and the solution diffusion models for the separation of binary and multi-component systems in reverse osmosis process. *Comput. Chem. Eng.* **2017**, *100*, 48–79. [CrossRef]

28. Water, D.; Solutions, P. *Filmtec Reverse Osmosis Membranes Technical Manual*; Dow Water and Process Solutions: Midland, MI, USA, 2005.

29. Ruiz-García, A.; Nuez, I. Long-term performance decline in a brackish water reverse osmosis desalination plant. Predictive model for the water permeability coefficient. *Desalination* **2016**, *397*, 101–107. [CrossRef]

30. Ruiz-García, A.; Melián-Martel, N.; Nuez, I. Short Review on Predicting Fouling in RO Desalination. *Membranes* **2017**, *7*, 62. [CrossRef]

31. Du, Y.; Xie, L.; Liu, J.; Wang, Y.; Xu, Y.; Wang, S. Multi-objective optimization of reverse osmosis networks by lexicographic optimization and augmented epsilon constraint method. *Desalination* **2014**, *333*, 66–81. [CrossRef]

32. Boudinar, M.; Hanbury, W.; Avlonitis, S. Numerical simulation and optimisation of spiral-wound modules. *Desalination* **1992**, *86*, 273–290. [CrossRef]

33. Ruiz-García, A.; de la Nuez-Pestana, I. A computational tool for designing BWRO systems with spiral wound modules. *Desalination* **2018**, *426*, 69–77. [CrossRef]